

Article

Corresponding States for Volumes of Elemental Solids at Their Pressures of Polymorphic Transformations

Oliver Tschauner 

Department of Geoscience, University of Nevada Las Vegas, Las Vegas, NV 89154, USA;
oliver.tschauner@unlv.edu

Abstract: Many non-molecular elemental solids exhibit common features in their structures over the range of 0 to 0.5 TPa that have been correlated with equivalent valence electron configurations. Here, it is shown that the pressures and volumes at polymorphic transitions obey corresponding states given by a single, empirical universal step-function $V_{tr}/L = -0.0208(3) \cdot P_{tr} + N_i$, where V_{tr} is the atomic volume in \AA^3 at a given transformation pressure P_{tr} in GPa, and L is the principal quantum number. N_i assumes discrete values of approximately 20, 30, 40, etc. times the cube of the Bohr radius, thus separating all 113 examined polymorphic elements into five discrete sets. The separation into these sets is not along L . Instead, strongly contractive polymorphic transformations of a given elemental solid involve changes to different sets. The rule of corresponding states allows for predicting atomic volumes of elemental polymorphs of hitherto unknown structures and the transitions from molecular into non-molecular phases such as for hydrogen. Though not an equation of state, this relation establishes a basic principle ruling over a vast range of simple and complex solid structures that confirms that effective single-electron-based calculations are good approximations for these materials and pressures. The relation between transformation pressures and volumes paves the way to a quantitative assessment of the state of very dense matter intermediate between the terrestrial pressure regime and stellar matter.

Keywords: corresponding states; high pressure; Wigner–Seitz radii; elemental solids; phase transformation



Citation: Tschauner, O.

Corresponding States for Volumes of Elemental Solids at Their Pressures of Polymorphic Transformations.

Crystals **2022**, *12*, 1698. <https://doi.org/10.3390/cryst12121698>

Academic Editors: Daniel Errandonea and Enrico Bandiello

Received: 1 November 2022

Accepted: 16 November 2022

Published: 23 November 2022

Publisher's Note: MDPI stays neutral with regard to jurisdictional claims in published maps and institutional affiliations.



Copyright: © 2022 by the author. Licensee MDPI, Basel, Switzerland. This article is an open access article distributed under the terms and conditions of the Creative Commons Attribution (CC BY) license (<https://creativecommons.org/licenses/by/4.0/>).

1. Introduction

In difference to gases whose states can be described by the ideal gas- or the van der Waals equations of state, solids seem to defy the concept of a general equation of state. The range of structures and properties as well as their changes upon compression appear too large to be comprised within a single formula. Over a range of pressure of 0 to 500 GPa, many elements that are molecular solids at ambient conditions transform into atomic metals [1], while others that are normal metals at ambient conditions become semiconductors [2–4], and some monatomic elemental solids assume complex structures under compression that do not exist at ambient pressure [5,6].

These changes are not arbitrary but reflect general trends in the effect of pressure on the valence electron structure of solid matter over large pressure intervals [1–12]. The changes in the valence electron configuration reflect the different response of different orbital states to the increase in electron density upon compression [2,7,10–15]. The atomic volume often is markedly reduced upon such transitions. The transition from the bcc to the hcp structure in many transition metal elements is correlated with an increase in the hybridization of filled d-states with p-states of the next higher principal quantum number [16,17]. Similarly, the pressure-induced transformations of lanthanides from hcp to the Sm type to dhcp to fcc is explained through the increased occupancy of valence d-states [11–13], whereas the marked volume collapse and transitions to low symmetric phases in lanthanides are assigned to delocalization of the 4f states [12,13,15]. A different type of delocalization occurs in the low-Z elemental alkaline metals, which at high pressure transform into electrides in which inner

shell electron states overlap with valence s-states and non-bonding p-states are occupied on expenses of the bonding s- and p-hybrid states [2,4,14]. As a consequence, elements such as Li and Na, which are normal metals at ambient conditions, become semiconductors at pressures between 100 and 200 GPa [2–4]. Changes in the electronic valence states have been studied quantitatively for some alkaline metals, transition group elements, and lanthanides through X-ray spectroscopy [10,14–17]. These changes are correlated with structural transformations. It has been noted that these pressure-induced valence changes follow general correlations of the nuclear charge number with the pressure, volume, and structure type [5,8–10]. In addition, there are correlations between the atomic volumes of equivalent polymorphs of different elements [8,18].

Here, it is shown that all known non-molecular elemental solids follow a rule of corresponding states if only the volumes and pressures at the polymorphic transitions are considered. This observation extends to high-pressure atomic polymorphs of elements that are molecular at ambient conditions, such as O, N, S, P, Cl, Br, and I. Only experimental data are considered here (see Section 2), hence the relation presented is without any kind of simplifying assumptions or theory.

2. Materials and Methods

Only published volumes and transformation pressures of polymorphs of elemental solids are used in this paper. Recently published data and work conducted under hydrostatic or nearly hydrostatic conditions are given preference. This includes data obtained from samples embedded in He or Ne as pressure media or data from crystals grown from melt at a high pressure. Data from compression experiments without pressure media are only included if the average pressure has been below 10 GPa. However, the induced transformations in Ir, Pb, and Th under non-hydrostatic stresses are included for reference. Similarly, compression data of some lanthanides are included due to their principal interest, although most of these data were not and possibly could not be acquired with the use of hydrostatic media. The plotted volumes V_{tr} and pressures P_{tr} at the polymorphic transitions are generally those of the first observation of a high-pressure polymorph upon compression at 300 K. In a few cases in which the transformations exhibits hysteresis larger than 5 GPa, the arithmetic middle pressure has been taken as P_{tr} . In all other cases, the hysteresis has been added to the uncertainty. For some elemental high-pressure polymorphs, the structures have been redetermined in more recent studies but without reassessment of the 300 K isotherms. In such cases, the atomic volume of the correct structure has been used to reassess the atomic volume at the pressure of the transformation that has been reported in the earlier studies. The complete data are given in Table 1 at the end of the paper.

3. Results

For all of the examined 113 elemental solids, the volume at the phase transition $V_{tr} = V(P_{tr})$ (P_{tr} = transition pressure) divided by the principal quantum number L exhibits a universal linear pressure dependence of $-0.0208(3) \cdot P_{tr}$ (P_{tr} in GPa; atomic volume in \AA^3 ; the adjusted R^2 of the linear fit was 0.9985; see Supplemental Figure S1). This is shown in Figure 1. Furthermore, within the uncertainties, the constant term of this equation provides a volume that for all of the examined elemental solids is nearly equal to $n \cdot 10 \cdot r_B^3$, where n is an integer number between 2 and 6, and r_B is the Bohr radius in \AA . This is shown in Figure 2. In other words:

$$V_{tr}/L + 0.0208(3) \cdot P_{tr} = N_i \approx n \cdot 10 \cdot r_B^3 \quad (1)$$

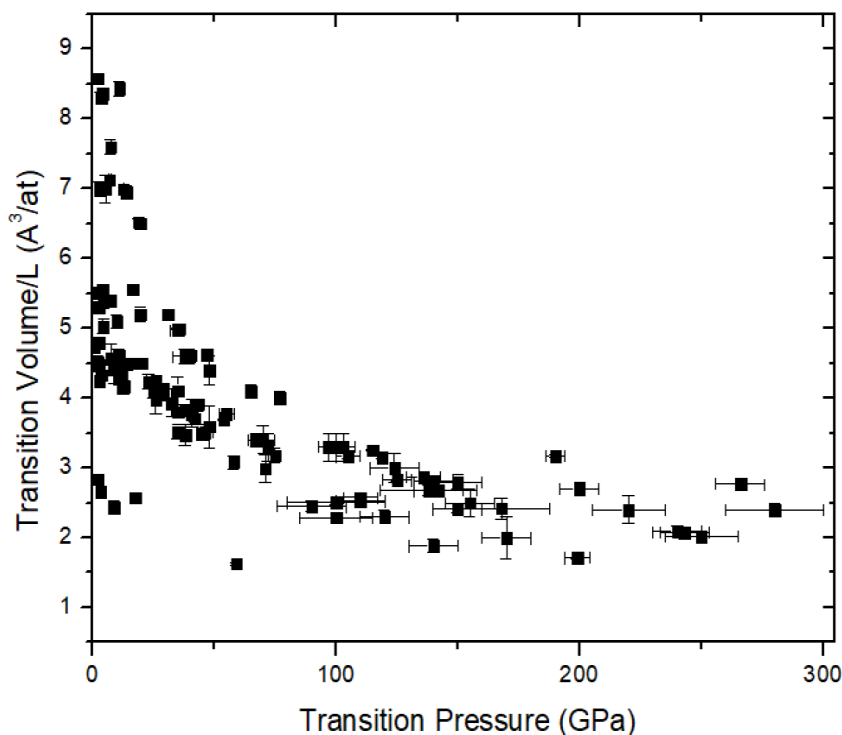


Figure 1. Volume of elemental polymorphs in Å³/at at 300 K divided by the principal quantum number L as a function of pressure in GPa. The volumes are those that are observed at the pressure of their formation through direct phase transformation from lower pressure polymorphs; the plotted pressures are the pressures of the transformation. The linear relation between these volumes and pressures and the existence of five distinct sets of pressure–volume relations is clearly visible.

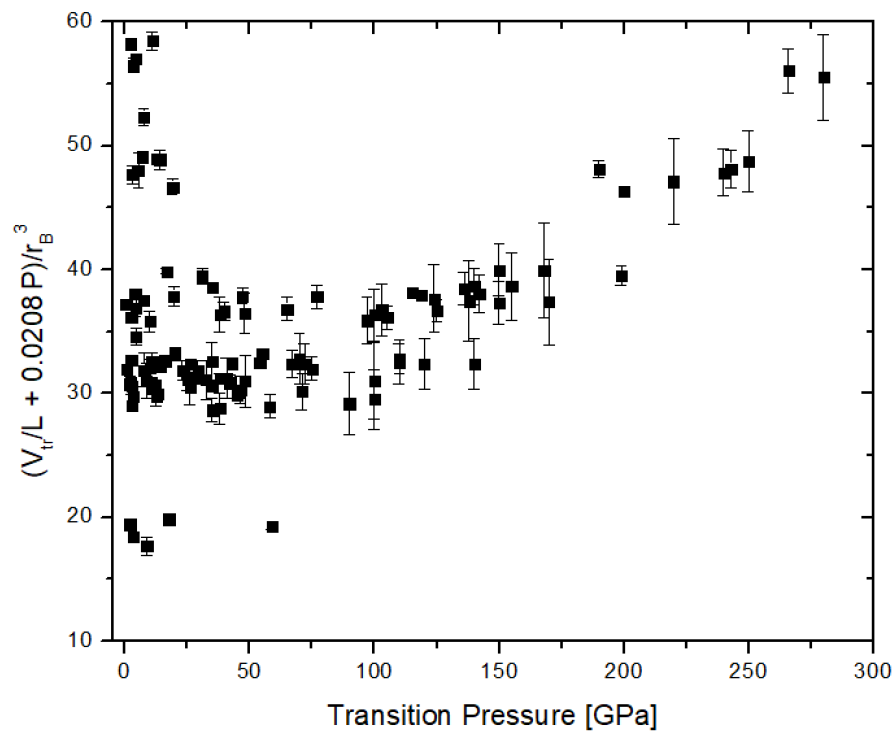


Figure 2. This figure shows the data from Figure 1 with the volume corrected for the linear pressure dependence from Equation (1). The remaining constant term of each set is approximately equal to integer multiples of 2, 3, 4, 5, and 6 of 10 times the cube of the Bohr radius.

The actual values of the five distinct volumes for N_i are 2.88(8), 4.58(4), 5.51(5), 7.14(5), 8.53(6) $\text{\AA}^3/\text{at}$, which is 19.5(4), 30.9(4), 37.2(8), 48.2(1), and 57.6(5) times the cube of the Bohr radius r_B^3 in \AA^3 , respectively. Therefore, Figures 1 and 2 show that the volumes of elemental solids at their polymorphic transitions assume corresponding states. It is important to recall that this universal relation of corresponding states only holds for the pressures and volumes at the phase transitions: Within the stability field of each polymorph, the pressure–volume relation is controlled by its specific compressibility that itself depends on pressure and temperature and that, in general, is far from being linear, universal, and discrete. Equation (1) is therefore not an equation of state.

4. Discussion

The ‘collective quantization’ shown in Figure 1 may, upon first glance, be assigned to the factorization by the principal quantum number L . However, the series of corresponding states N_i does not follow the rows of the periodic table. Rather, many elements with subsequent polymorphic transitions change between states N_i . For instance, the high-pressure polymorphs fcc, c16, and oc120 of Na reside in $N_4 = 5.51(5) \text{\AA}^3/\text{at} \approx 40 \cdot r_B^3$ along with K-IV, Rb-IV, -V, Cs-IV, and Ca-III to -IV; whereas the hp4-type Na resides in $N_5 = 7.14(5) \text{\AA}^3/\text{at} \approx 50 \cdot r_B^3$ along with Rb-II and -III. In some cases, for instance Si, all polymorphs remain within one set N_i ; however, for most elements at least some polymorphs fall into different sets. For instance, Cs-II and Cs-III are in N_6 but Cs-IV and -V belong to N_4 and Cs-VI to N_3 . A sequence of stepwise transitions to sets with a lower state N_i along with an increasing transformation pressure is found for many elements: the high-pressure polymorphs of Rb fall into the sets N_5 (Rb-II and -III), N_4 (Rb-IV, -V, -VIII), and N_3 (Rb-VI, -VII); Li into N_6 (Li-II), N_4 (Li-III, -IV, -VI), and N_3 (Li-V); and the various polymorphs of the alkaline earths Ca, Sr, and Ba are found in the sets N_3 to N_6 (Figures 1 and 2), where the higher pressure polymorphs belong to sets with a smaller N_i . Lower sets N_i have markedly smaller volumes at a given pressure than the corresponding higher sets N_{i+1} (Figure 1), and the polymorphic transitions that involve changes $N_i \rightarrow N_{i-1}$ are accompanied by marked volume contractions $(V_{\text{tr}}^{\text{LP}} - V_{\text{tr}}^{\text{HP}})/V_0$ where $V_{\text{tr}}^{\text{LP}}$ and $V_{\text{tr}}^{\text{HP}}$ are the atomic volumes of the low- and the high-pressure polymorphs, respectively, at the pressure of the phase transitions; and V_0 is the volume of the ambient pressure phase at standard conditions. A smaller number of elements also exhibit transitions into higher sets N_{i+1} at higher pressure. In particular, this holds for the polymorphic transitions to Sc-V [19], bcc-Ti [20,21], hp4-Na [3], and Rb-VIII (Figure 1), but also for the elastic anomaly of Os around 290 GPa [22], which is taken here for an isostructural transition. There is a simple reason for these ‘upward transitions’ $N_i \rightarrow N_{i+1}$: at the given transformation pressure, the corresponding volumes of the next lower set N_{i-1} would be negative. It is to be expected that for all elements at sufficiently high pressures, the cascade of successive, markedly contractive transitions $N_i \rightarrow N_{i-1}$ is followed by transitions $N_i \rightarrow N_{i+1}$ to polymorphs in higher sets with a less pronounced contraction once $N_i \rightarrow N_{i-1}$ reaches the limit of negative volumes. Transitions to higher sets come with smaller contractions $(V_{\text{tr}}^{\text{LP}} - V_{\text{tr}}^{\text{HP}})/V_0$ than those into lower sets.

4.1. Theoretical Explanation

‘Upward’ and ‘downward’ transitions between different states N_i can be correlated to changes in the valence electron configuration wherever such information has been obtained experimentally [10,15,17] or through calculation [14]. The fact that the volumes N_i are nearly equal to integer multiples of r_B^3 has a straightforward theoretical basis: It implies that the volumes that occur at polymorphic transitions of non-molecular elements are controlled by the number of valence electrons rather than by their interactions. Besides the limited experimental accuracy the electron exchange- and Coulomb interactions account for part of the deviations from Equation (1) and from integer N_i values; thus, the interaction terms are of the second order with respect to the volumes. In other words, Equation (1) is the equivalent to an ideal equation of state for elemental solids, only that it does not describe

continuous pressure–volume changes but discrete changes that occur at the phase transitions. This finding can be further quantified by considering the effect of the different valence orbital states as based on the experimentally determined pressure-induced hybridization of d-states of the alkaline metals Rb, Cs, and K (the latter element exhibits no measurable d-state occupancy up to 40 GPa) [10]. Figure 1 may be re-parametrized in terms of pressure-induced changes in the d-state occupancy at the valence level. In particular, the d-state occupancy of the elemental polymorphs can be correlated with the five sets N_2 to N_6 shown in Figure 1 through their 0 GPa intercepts. This is shown in Figure 3a. For instance, the d-state occupancy of Cs increases for phase Cs-II to -VI from ~ 0.0 to ~ 0.6 , and for Rb from ~ 0.2 to 0.4 electrons between Rb-II and -VI [10]. The high-P polymorphs of Li and Na have little or no occupied d-states in this diagram and according to earlier computational work [2,4,14]. The correlation between $\Delta n(d)$ and N_i is linear, at least for the polymorphs K-II, Rb-II,-IV, Cs-II, and Cs-III (black squares in Figure 3a): Within uncertainty, the slopes are equal for all sets. In terms of multiples of the electron elemental charge, this linear correlation between d-state occupancy, V_{tr} , and L is:

$$N_i = N_i^0 - 6.11(14) \cdot 10^{-11} \cdot n(d) \cdot e \quad (2)$$

where $N_i^0 = N_i$ at $n(d) = 0$, the constant factor is given in $m^3/(C \cdot at)$, and e is the electron elemental charge. However, the correlation between N_i and $n(d)$ is not continuous: Equations (1) and (2) can be combined to give:

$$\frac{V_{tr}}{L} = -2.08(3) \cdot 10^{-32} \cdot P - 6.11(14) \cdot 10^{-11} \cdot \sum_{i=0}^{m-1} i \cdot n(d) \cdot e + N_m \quad (3)$$

where N_m is the value assumed at $n(d) = 0$, P is in GPa, V is in m^3/at , and e is the electron elemental charge. The effect of the $d \rightarrow p$ transfer on shifts into sets with a higher N_i has been discussed above. Overall, there are fewer data on pressure-induced changes in the valence p-state occupancy (summarized in Supplementary Figure S2, see refs. [10,16,17]), but within uncertainties, the relation between V_{tr}/L and $n(p)$ has the same slope as in (3) but with an opposed sign (consistent with the transfer into higher sets N_i , whereas changes in the d-state occupancy generally result in changes to a lower N_i). Implementing $n(p)$ into (3), dividing through r_B^3 , and using the approximation $N_i r_B^3 \sim 10 \cdot m$ gives:

$$\begin{aligned} \frac{V_{tr}}{L \cdot r_B^3} &= -0.1405(20) \cdot P + 10 \cdot m - 66.1(15) \cdot \sum_{i=0}^{m-1} i \cdot 0.15(4) + 66(2) \cdot \sum_{j=p}^m j \cdot \\ 0.09(21) &= -0.1405(20) \cdot P + 10 \cdot m - 10.0(6) \cdot \sum_{i=0}^{m-1} i + 6(1) \cdot \sum_{j=p}^m j \end{aligned} \quad (4)$$

where the pressure is given in GPa, the volumes N_i are taken as integer multiples $10 \cdot i \in \mathbb{IN}$ (the set of natural numbers) of r_B^3 per atom, $p \leq n(d)$, and the increments $\Delta n(d)$ are taken as 0.151 ; hence: $66.1 \cdot 0.151 = 10$ d-electrons and accordingly $66(2) \cdot 0.09(1) = 6(1)$ for the p-electrons. Thus, within uncertainties, the factors of the sum terms equal the number of p- and d-states and an additional term for f-electrons with factor -14 may be added. The actual values N_i may be substituted for $10m$.

The volumes of elemental atomic solids at ambient conditions are not bound to Equation (1) because they do not represent volumes at phase transitions. However, the correlation $V = N_i \cdot L$ is within $\pm 10\%$ of the observed volumes at ambient conditions for 28 and within 20% for 38 out of the 42 non-molecular solid elements (Figure 3b). Considering that the atomic volumes of elemental metals are equal to the cube of the Wigner–Seitz radii, their approximate relation to $N_i \cdot L$ is equivalent to a relation recently found for the ionic radii [23]. However, in the present case of elemental solids the relation does not rely on any approximate model of bonding.

and the V_{tr} of the intermediate phase IV (i-oF3, [29]) falls in between $V_{tr}/L + N_5$ and $V_{tr}/L + N_6$. The isotherms of N, S, P, Br, and I all intersect the trajectories $V_{tr}/L + N_i$ at the pressures of the observed transitions to non-molecular phases [8,27,30,31] and fall mostly below the ‘molecular gap’ because their transitions to non-molecular solids occur at lower pressure.

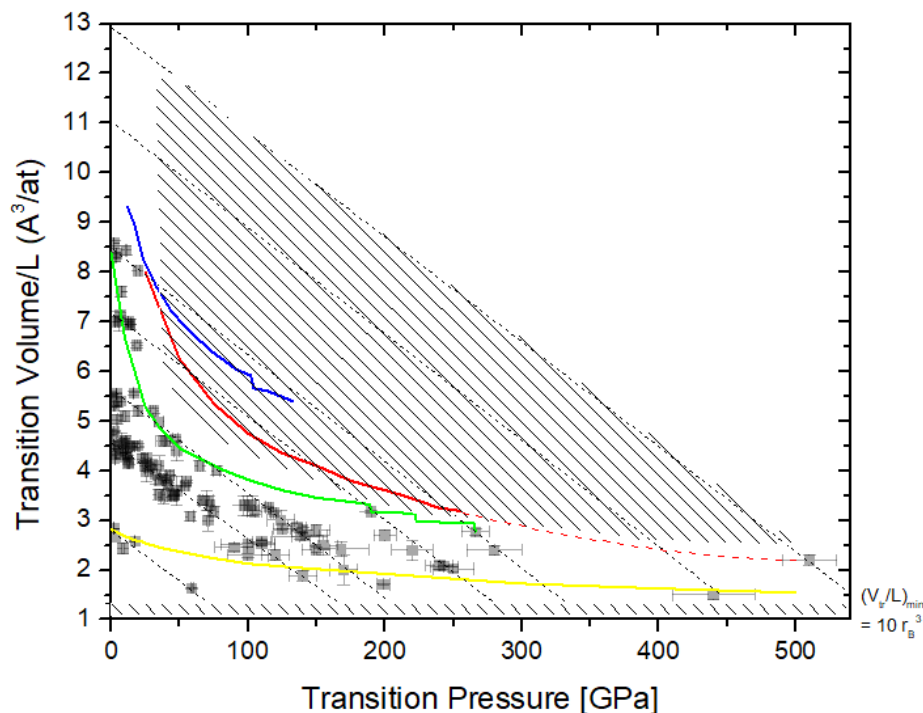


Figure 4. Data from Figure 1 with the equations of state for gold [24], chlorine [29], hydrogen [27], and oxygen [26] shown as yellow, green, red, and blue lines, respectively. Dashed lines indicate the distinct sets that defined V_{tr}/L versus P as defined by Equation (1). The additional data points for hydrogen [32] and the second elastic anomaly of osmium [22] have been added. Hatched areas mark the molecular gap and the forbidden zone below $V_{tr}/L = 10 \cdot r_B^3$.

Interestingly, the extrapolated pressure of the direct gap closure of H_2 that has been assessed through inelastic X-ray spectroscopy of H_2 [32] matches the intersection of the extrapolated isotherm of H_2 [27] and a trajectory $V_{tr}/L + N_9$ (of 13.0 to $13.3 \text{ \AA}^3/\text{at} = 90 r_B^3$ by using the intersection of the trajectory N_9 in Figures 3a and 4) at around 0.5 TPa , which suggests that the transition from molecular to atomic hydrogen occurs at that pressure at 300 K .

Finally, it is noticed that Equation (1) could be used to assess the atomic volumes of polymorphs with extant structure analyses such as Ca-VII, Sc-III and -IV, Ga-IV, and metastable Ir-II to $8.0(5)$, $12.08(8)$, $10.3(11)$, $9.2(4)$, and $9.78(12) \text{ \AA}^3/\text{at}$ at 170 , 26 , 35 , 120 , and 59 GPa , respectively (Table 1). The volume of hydrogen at the predicted transition at $490\text{--}530 \text{ GPa}$ is estimated to $2.3(2) \text{ \AA}^3/\text{at}$. This and above values (marked with an asterisk) and the entire list of volumes V_{tr} and pressures P_{tr} are given in Table 1.

Table 1. Columns from left to right: Name of polymorph, pressure of phase transition at 300 K , volume of phase transition divided by the principal quantum number L , volume of phase transition at 300 K , and reference(s).

| Phase | P_{tr} [GPa] | V_{tr}/L [$\text{\AA}^3/\text{at}$] | V_{tr} [$\text{\AA}^3/\text{at}$] | Reference(s) |
|--------|----------------|---|---------------------------------------|--------------|
| Li-fcc | 7.5(1) | 7.6(1) | 15.2(2) | [33–35] |
| Li-hR1 | 39.7(1.0) | 4.6(1) | 9.2(2) | [34,36] |
| Li-c16 | 48(2) | 4.4 | 8.8(4) | [34,35] |

Table 1. Cont.

| Phase | P_{tr} [GPa] | V_{tr}/L [$\text{\AA}^3/\text{at}$] | V_{tr} [$\text{\AA}^3/\text{at}$] | Reference(s) |
|---------------------------|----------------|---|---------------------------------------|--------------|
| Li-oC40 | 67(2) | 3.4(1) | 6.8(2) | [35] |
| Li-oC24 | 97(3) | 3.3(2) | 6.6(4) | [35] |
| Na-fcc | 67(1) | 4.10(5) | 12.3(30) | [36] |
| Na-cl16 | 115(2) | 3.26(1) | 9.77(3) | [3] |
| Na-oP8 | 119(2) | 3.15(1) | 9.45(6) | [3] |
| Na-h4p | 200(8) | 2.7(1) | 8.1(3) | [2] |
| K-fcc | 11.0(5) | 8.4(1) | 33.74(4) | [37] |
| K-III | 22(43) | 5.64(5) | 22.57(3) | [5] |
| K-IIIb | 31(2) | 5.2(2) | 20.8(4) | [38] |
| K-IV (oP8) | 54(2) | 3.69(1) | 14.78(4) | [39] |
| Rb-II | 7.0(5) | 7.13(6) | 35.65(30) | [37] |
| Rb-III | 14.3(2) | 6.95(1) | 34.77(5) | [5] |
| Rb-IV | 16.7(1) | 5.56(1) | 27.8(15) | [5,40] |
| Rb-V | 19.6(5) | 5.2(1) | 26.0(5) | [41] |
| Rb-VI | 48.1(5) | 3.6(3) | 18.0(1.5) | [41] |
| Rb-VII | >70 | 3.4(1) | 17(1) | [41] |
| Rb-VIII | 220(15) | 2.4(1) | 12(1) | [41] |
| Cs-II | 2.37(1) | 8.58(1) | 51.47(6) | [42] |
| Cs-III | 4.20(2) | 8.37(1) | 50.22(6) | [5] |
| Cs-IV | 4.30(2) | 5.83(1) | 32.28(6) | [43] |
| Cs-V | 10(1) | 5.1(2) | 30.6(1.2) | [44] |
| Cs-VI | 72(2) | 2.6(2) | 15.6(1.2) | [44,45] |
| Mg-bcc | 47(2) | 4.63(3) | 13.9(2) | [46] |
| Ca-II | 19.5(15) | 8.02(2) | 32.08(8) | [47,48] |
| Ca-III | 35(3) | 5.0(1) | 19.9(4) | [49,50] |
| Ca-IV | 124(10) | 3.0(2) | 12.0(8) | [50] |
| Ca-V/VI | 155(15) | 2.5(2) | 10.0(8) | [50] |
| Ca-VII | 170 * | 2.0 * | 8 | this work |
| Sr-II | 3.5(2) | 8.30(8) | 41.5(4) | [48] |
| Sr-III | 26.0(6) | 3.98(19) | 19.9(9) | [5,49] |
| Sr-IV | 35(1) | 4.1(2) | 20.5(10) | [5,49,51] |
| Sr-V | 46(3) | 3.5(1) | 17.5(5) | [5,49,51] |
| Ba-II | 5.5(1) | 7.14(4) | 42.84(24) | [48] |
| Ba-IV | 12.6(1) | 7.0(1) | 42.0(6) | [52] |
| Ba-V | 45(2) | 3.5(1) | 21.0(6) | [53] |
| Sc-II | 20(1) | 4.5(1) | 18.0(4) | [54] |
| Sc-III | 104(5) | 3.02(2) * | 12.08(8) | [54] |
| Sc-IV | 140(10) | 2.58(27) * | 10.3(1.1) | [54] |
| Sc-V | 240(10) | 2.09(7) | 3.36(28) | [19] |
| ω -Zr | 12.5(10) | 4.15(5) | 20.75(25) | [55] |
| Zr-bcc | 35(2) | 3.5(10) | 17.5(50) | [55,56] |
| Zr-bccII | 58–60 | 3.08(5) | 15.4(3) | [55] |
| ω -Ti | 0(5) | 4.375(15) | 17.5(6) | [20] |
| γ -Ti | 110(10) | 2.55(5) | 10.2(2) | [20,21] |
| δ -Ti | 150(10) | 2.41(5) | 9.64(20) | [20,21] |
| Ti-bcc | 243(10) | 2.07(3) | 8.28(12) | [21] |
| $V_{\text{rhombohedral}}$ | 250(20) | 2.02(5) | 8.08(20) | [57] |
| Fe-hcp | 17.6(1) | 2.57(1) | 10.28(4) | [58] |
| Os-hcpII | 140(10) | 1.88(10) | 11.28(60) | [22] |
| Os-hcpIII | 440(20) | 1.5(1) | 9.0(6) | [22] |
| Sn-bct | 10.8(1) | 4.60(1) | 23.00(5) | [59] |
| Sn-bco | 32.5(10) | 3.93(1) | 19.65(5) | [59] |
| Sn-bcc | 40.8(15) | 3.78(1) | 18.9(5) | [59] |
| Pb-hcp | 14(1) | 6.95(10) | 41.7(6) | [60] |
| Pb-bcc | 142(10) | 2.68(2) | 16.08(12) | [5,61] |
| Ga-II | 2.0(2) | 4.52(8) | 18.08(32) | [5] |
| Ga-III | 2.8(1) | 4.24(5) | 16.96(24) | [62] |
| Ga-V | 10.5(2) | 4.358(5) | 17.432(24) | [5] |
| Ga-IV | 120(10) | 2.3(1)* | 9.2(4) | [62,63] |
| Tl-fcc | 3.5(5) | 4.3(2) | 25.8(1.2) | [64] |
| Ge-II | 10.6 | 4.28(8) | 17.12(32) | [65] |
| Ge-hp | 75(3) | 3.18(10) | 17.72(40) | [18,66] |
| Ge-Cmca | 140(120–160) * | 2.68(7) | 10.72(28) | [66] |
| Ge-hcp | >170 | 2.4(1) | 9.6(4) | [18] |
| Diamond | 2.0(1) | 2.837(1) | 5.674(2) | [67] |
| Si-II | 12(1) | 4.3(1) | 12.9(3) | [68] |
| Si-V | 16(2) | 4.43(2) | 13.29(6) | [69] |
| Si-VI | 38(2) | 3.83(1) | 11.49(3) | [69] |
| Si-VII | 42(2) | 3.71(2) | 11.13(6) | [69] |

Table 1. Cont.

| Phase | P_{tr} [GPa] | V_{tr}/L [$\text{\AA}^3/\text{at}$] | V_{tr} [$\text{\AA}^3/\text{at}$] | Reference(s) |
|--------------|----------------|---|---------------------------------------|--------------|
| N, cg-phase | 110(7) | 2.58(3) | 5.16(6) | [28] |
| P-A7 | 4.5(1) | 5.03(5) | 15.09(15) | [70] |
| P-sc | 10(1) | 4.54(2) | 13.62(6) | [70] |
| P-ph | 140(8) | 2.8(1) | 8.4(3) | [70] |
| P-bcc | 280(20) | 2.4(1) | 7.2(3) | [70] |
| As-sc | 25(1) | 4.1(1) | 16.4(4) | [18] |
| As-III | 46(3) | 3.5(1) | 14.0(4) | [18] |
| As-IV | 125(10) | 2.84(2) | 11.36(8) | [18] |
| Sb-II | 8.6(2) | 4.42(20) | 22.1(1) | [71] |
| Sb-V | 28(3) | 4.05(6) | 20.25(30) | [71] |
| Bi-II | 2.55(1) | 5.30(2) | 31.80(12) | [8] |
| Bi-III | 2.70(1) | 4.48(9) | 26.88(54) | [8] |
| Bi-V | 7.7(1) | 4.57(10) | 27.42(60) | [8] |
| S-II | 3.0(2) | 7.0(1) | 21.0(3) | [72] |
| S-III | 38(2) | 4.6(1) | 13.8(3) | [72] |
| S-IV | 103(6) | 3.3(1) | 9.9(3) | [72] |
| S-V | 150(10) | 2.8(1) | 8.4(3) | [72] |
| Se-VII | 14(1) | 4.5(1) | 18.0(4) | [72] |
| Se-III | 26(1) | 4.25(7) | 17.0(3) | [72] |
| Se-IV | 35(1) | 3.8(1) | 15.2(4) | [72] |
| Se-V | 77(2) | 4.0(1) | 16.0(4) | [72] |
| Se-VI | 136(7) | 2.87(7) | 11.48(28) | [18] |
| Te-II | 4.0(1) | 5.56(1) | 27.80(5) | [5,73] |
| Te-III | 7.4(1) | 5.40(1) | 27.00(5) | [5,73] |
| Te-V | 29.2(7) | 4.25(2) | 21.25(10) | [5,73] |
| Te-VI | 102(5) | 3.3(2) | 16.5(1) | [74] |
| I-bct | 43(3) | 3.9(1) | 19.6(1) | [75,76] |
| I-fcc | 55(4) | 3.78(2) | 18.9(1) | [75,76] |
| Th-bct | 100(30) | 2.51(1) | 17.57(7) | [77] |
| γ -Ce | 0.5(1) | 4.70(1) | 28.20(6) | [78] |
| PrtI2 | 180(10) | | 23.90(14) | [79] |
| Sm-dhcp | 0.4(1) | 5.51(1) | 33.06(6) | [80] |
| Sm-hR9 | 13(1) | 4.2(1) | 25.2(6) | [81] |
| Sm-oF8 | 90(10) | 2.45(8) | 14.70(48) | [81] |
| Nd-oF8 | 100(10) | 2.30(4) | 13.80(24) | [82] |
| Eu_IV | 31.5(20) | 3.32(2) | 19.9(1) | [83] |
| Gd-dhcp | 9(3) | 4.3(1) | 26 | [84] |
| Gd-fcc | 26(2) | 3.7(1) | 22.2(6) | [85] |
| Gd-dfcc | 33(2) | 3.43(10) | 20.5(6) | [85] |
| Gd-VIII | 60.5(3) | 2.86(10) | 17.15(61) | [85] |
| Dy-hR9 | 2.5(2) | 4.79(1) | 28.74(6) | [86] |
| Cl-IV | 266(10) | 2.77(6) | 8.31(18) | [29] |
| Ir-II | 59 | 1.63(2)* | 9.78(12) | [5,87] |

* Parameters calculated using Equation (1).

5. Conclusions

The volume and pressure of phase transformations of non-molecular elemental solids obeyed a universal relation of discrete corresponding states. These states, as defined in Equation (1), were close to integer multiples of the cube of the Bohr radius. Therefore, the volumes and pressures of polymorphic transitions of these solids were controlled by the number of valence electrons as specified in Equation (4). This finding was in accordance with the commonly used effective single-electron-based computational approaches for modeling elemental solids within the range of 0 to 0.5 TPa. However, Equation (1) can be used for constraining elemental metal volumes for first-principal- and empirical-potential-based calculations, thus removing the weakest point in these approaches (the proper assessment of volumes). The volumes of polymorphs at the phase transitions exhibited a general linear dependence on the pressure of the transition (see Equation (1)). Though not an equation of state, this relation establishes a very simple principle that rules over a vast range of simple and complex solid structures and a range of pressure of 0.5 TPa.

Funding: This research received no external funding.

Supplementary Materials: The following supporting information can be downloaded at: <https://www.mdpi.com/article/10.3390/cryst12121698/s1>, Figure S1: Volume of elemental polymorphs in Å³/at divided by the principal quantum number L as function of pressure in GPa and mapped onto the set N₄; Figure S2: Correlation between the normalized transformation volumes from Equation (1) and p-state occupancy.

Data Availability Statement: All data are provided in the paper.

Acknowledgments: Comments and suggestions by S. Huang, H.-k. Mao, A. Zerr, and by two anonymous reviewers are gratefully acknowledged.

Conflicts of Interest: The author declares no conflict of interest.

References

1. Mao, H.-K.; Chen, X.J.; Ding, Y.; Li, B.; Wang, L. Solids, liquids, and gases under high pressure. *Rev. Mod. Phys.* **2018**, *90*, 015007. [[CrossRef](#)]
2. Ma, Y.M.; Eremets, M.; Oganov, A.R.; Xie, Y.; Trojan, I.; Medvedev, S.; Lyakhov, S.; Valle, M.; Prakapenka, V. Transparent dense sodium. *Nature* **2009**, *458*, 182–185. [[CrossRef](#)] [[PubMed](#)]
3. Gregoryanz, E.; Lundegaard, L.F.; McMahon, M.I.; Guillaume, C.; Nelmes, R.J.; Mezouar, M. Structural diversity of sodium. *Science* **2009**, *320*, 1054–1057. [[CrossRef](#)]
4. Marques, M.; McMahon, M.I.; Gregoryanz, E.; Hanfland, M.; Guillaume, C.L.; Pickard, C.J.; Ackland, G.J.; Nelmes, R.J. Crystal Structures of Dense Lithium: A Metal-Semiconductor-Metal Transition. *Phys. Rev. Lett.* **2011**, *106*, 095502. [[CrossRef](#)] [[PubMed](#)]
5. McMahon, M.I.; Nelmes, R.J. High-pressure structures and phase transformations in elemental metals. *Chem. Soc. Rev.* **2006**, *35*, 943–963. [[CrossRef](#)]
6. Schwarz, U. High-pressure crystallography and synthesis. *Z. Krist.* **2004**, *219*, 943–963.
7. Cammi, R.; Rahm, M.; Hoffmann, R.; Ashcroft, N.W. Varying Electronic Configurations in Compressed Atoms: From the Role of the Spatial Extension of Atomic Orbitals to the Change of Electronic Configuration as an Isobaric Transformation. *J. Chem. Theory Comput.* **2020**, *16*, 5047–5056. [[CrossRef](#)]
8. Degtyareva, O.; McMahon, M.I.; Nelmes, R.J. High-pressure structural studies of group 1-5 elements. *High Press. Res.* **2004**, *24*, 319–356. [[CrossRef](#)]
9. Winzenick, M.; Vijayakumar, V.; Holzapfel, W.B. High-pressure X-ray-diffraction on potassium and rubidium up to 50 GPa. *Phys. Rev. B* **1994**, *50*, 12381–12385. [[CrossRef](#)] [[PubMed](#)]
10. Fabbris, G.; Lim, J.; Veiga, L.S.I.; Haskel, D.; Schilling, J.S. Electronic and structural ground state of heavy alkali metals at high pressure. *Phys. Rev. B* **2015**, *91*, 085111. [[CrossRef](#)]
11. Duthie, J.C.; Pettifor, D.G. Correlation between d-band occupancy and crystal-structure in rare-earths. *Phys. Rev. Lett.* **1977**, *38*, 564–567. [[CrossRef](#)]
12. Holzapfel, W.B. Structural systematics of 4f and 5f elements under pressure. *J. Alloys Comp.* **1995**, *224*, 319–356. [[CrossRef](#)]
13. Eriksson, O.; Brooks, M.S.S.; Johansson, B. Orbital polarization in narrow-band systems—Application to volume collapses in light lanthanides. *Phys. Rev. B* **1990**, *41*, 7311–7314. [[CrossRef](#)]
14. Neaton, J.B.; Ashcroft, N.W. On the constitution of sodium at higher densities. *Phys. Rev. Lett.* **2001**, *86*, 2830–2833. [[CrossRef](#)] [[PubMed](#)]
15. Bradley, J.A.; Moore, K.T.; Lipp, M.J.; Mattern, B.A.; Pacold, J.I.; Seidler, G.T.; Chow, P.; Rod, E.; Xiao, Y.M.; Evans, W.J. 4f electron delocalization and volume collapse in praseodymium metal. *Phys. Rev. B* **2021**, *85*, 100102. [[CrossRef](#)]
16. Iota, V.; Klepeis, J.H.P.; Yoo, C.S.; Lang, J.; Haskel, D.; Srajer, G. Electronic structure and magnetism in compressed transition metals. *Appl. Phys. Lett.* **2007**, *90*, 042505. [[CrossRef](#)]
17. Dewaele, A.; Stutzmann, V.; Bouchet, J.; Bottin, F.; Occelli, F.; Mezouar, M. The $\alpha \rightarrow \omega$ phase transformation in zirconium followed with ms-scale time-resolved X-ray absorption spectroscopy. *High Press. Res.* **2016**, *36*, 237–249.
18. Akahama, Y.; Kamiue, K.; Okawa, N.; Kawaguchi, S.; Hirao, N.; Ohishi, Y. Volume compression of period 4 elements: Zn, Ge, As, and Se above 200GPa: Ordering of atomic volume by atomic number. *J. Appl. Phys.* **2021**, *129*, 02590. [[CrossRef](#)]
19. Akahama, Y.; Fujihisa, H.; Kawamura, H. New helical chain structure for scandium at 240 GPa. *Phys. Rev. Lett.* **2005**, *94*, 195503. [[CrossRef](#)] [[PubMed](#)]
20. Dewaele, A.; Stutzmann, V.; Bouchet, J.; Bottin, F.; Occelli, F.; Mezouar, M. High pressure-temperature phase diagram and equation of state of titanium. *Phys. Rev. B* **2015**, *91*, 134108. [[CrossRef](#)]
21. Akahama, Y.; Kawaguchi, S.; Hirao, N.; Ohishi, Y. Observation of high-pressure bcc phase of titanium at 243GPa. *J. Appl. Phys.* **2020**, *128*, 035901. [[CrossRef](#)]
22. Dubrovinsky, L.; Dubrovinskaja, N.; Bykova, E.; Bykov, M.; Prakapenka, V.; Prescher, C.; Glazyrin, K.; Liermann, H.-P.; Hanfland, M.; Ekholm, M.; et al. The most incompressible metal osmium at static pressures above 750 gigapascals. *Nature* **2015**, *525*, 226–228. [[CrossRef](#)] [[PubMed](#)]

23. Tschauner, O. Observations about the pressure-dependence of ionic radii. *Geoscience* **2022**, *12*, 246. [[CrossRef](#)]
24. Anzellini, S.; Dewaele, A.; Occelli, F.; Loubeyre, P.; Mezouar, M. Equation of state of rhenium and application for ultra high pressure calibration. *J. Appl. Phys.* **2014**, *115*, 043511. [[CrossRef](#)]
25. Fratanduono, D.E.; Millot, M.; Braun, D.G.; Ali, S.J.; Fernandez-Pañella, A.; Seagle, C.T.; Davis, J.-P.; Brown, J.L.; Akahama, Y.; Kraus, R.G.; et al. Establishing gold and platinum standards to 1 Terapascal using shockless compression. *Science* **2021**, *372*, 1063–1068. [[CrossRef](#)]
26. Weck, G.; Desgreniers, S.; Loubeyre, P.; Mezouar, M. Single-Crystal Structural Characterization of the Metallic Phase of Oxygen. *Phys. Rev. Lett.* **2009**, *102*, 255503. [[CrossRef](#)]
27. Cheng, J.; Li, B.; Liu, W.; Smith, J.S.; Majumdar, A.; Luo, W.; Ahuja, R.; Shu, J.; Wang, J.; Sinogeikin, S.; et al. Ultrahigh-pressure isostructural electronic transitions in hydrogen. *Nature* **2019**, *573*, 558–562.
28. Eremets, M.I.; Gavriluk, A.G.; Trojan, I.A.; Dzivenko, D.A.; Boehler, R. Single-bonded cubic form of nitrogen. *Nat. Mater.* **2004**, *3*, 558–563. [[CrossRef](#)] [[PubMed](#)]
29. Dalladay-Simpson, P.; Binns, J.; Pena-Alvarez, M.; Donnelly, M.E.; Greenberg, E.; Prakapenka, V.; Chen, X.J.; Gregoryanz, E.; Howie, R.T. Band gap closure, incommensurability and molecular dissociation of dense chlorine. *Nat. Commun.* **2019**, *10*, 1134. [[CrossRef](#)] [[PubMed](#)]
30. Fujihisa, H.; Fujii, Y.; Takemura, K.; Shimomura, O. Structural aspects of dense solid halogens under high-pressure studied by X-ray diffraction—Molecular dissociation and metallization. *J. Phys. Chem. Solids* **1995**, *56*, 1439–1444. [[CrossRef](#)]
31. Akahama, Y.; Miyakawa, M.; Taniguchi, T.; Sano-Furukawa, A.; Machida, S.; Hattori, T. Structure refinement of black phosphorus under high pressure. *J. Chem. Phys.* **2020**, *153*, 104704. [[CrossRef](#)] [[PubMed](#)]
32. Li, B.; Ding, Y.; Kim, D.Y.; Wang, L.; Weng, T.-C.; Yang, W.; Yu, Z.; Ji, C.; Wang, J.; Shu, J.; et al. Probing the Electronic Band Gap of Solid Hydrogen by Inelastic X-ray Scattering up to 90 GPa. *Phys. Rev. Lett.* **2021**, *126*, 036402. [[CrossRef](#)]
33. Hanfland, M.; Loa, I.; Syassen, K.; Schwarz, U.; Takemura, K. Equation of state of lithium to 21 GPa. *Solid State Commun.* **1999**, *112*, 123–127. [[CrossRef](#)]
34. Hanfland, M.; Syassen, K.; Christensen, N.E.; Novikov, D.L. New high-pressure phases of lithium. *Nature* **2000**, *408*, 175–178. [[CrossRef](#)] [[PubMed](#)]
35. Guillaume, C.L.; Gregoryanz, E.; Degtyareva, O.; McMahon, M.I.; Hanfland, M.; Evans, S.; Guthrie, M.; Sinogeikin, S.V.; Mao, H.-K. Cold melting and solid structures of dense lithium. *Nat. Phys.* **2011**, *7*, 211–214. [[CrossRef](#)]
36. Hanfland, M.; Loa, I.; Syassen, K. Sodium und pressure: Bcc to fcc structural transition and pressure-volume relation to 100 GPa. *Phys. Rev. B* **2002**, *65*, 184109. [[CrossRef](#)]
37. Olijnyk, H.; Holzapfel, W.B. Phase transitions in K and Rb under pressure. *Phys. Lett.* **1983**, *99A*, 381–383. [[CrossRef](#)]
38. Lundegaard, L.F.; Stinton, G.W.; Zelazny, M.; Guillaume, C.L.; Proctor, J.E.; Loa, I.; Gregoryanz, E.; Nelmes, R.J.; McMahon, M.I. Observation of a reentrant phase transition in incommensurate potassium. *Phys. Rev. B* **2013**, *88*, 054106. [[CrossRef](#)]
39. Lundegaard, L.F.; Marques, M.; Stinton, G.; Ackland, G.J.; Nelmes, R.J.; McMahon, M.I. Observation of the oP8 crystal structure in potassium at high pressure. *Phys. Rev. B* **2009**, *80*, 020101. [[CrossRef](#)]
40. Schwarz, U.; Grzechnik, A.; Syassen, K.; Loa, I.; Hanfland, M. Rubidium-IV: A high pressure phase with complex crystal structure. *Phys. Rev. Lett.* **1999**, *83*, 4085–4088. [[CrossRef](#)]
41. Storm, C.V.; McHardy, J.D.; Finnegan, S.E.; Pace, E.J.; Stevenson, M.G.; Duff, M.J.; MacLeod, S.G.; McMahon, M.I. Behavior of rubidium at over eightfold static compression. *Phys. Rev. B* **2021**, *103*, 224103. [[CrossRef](#)]
42. Hall, H.T.; Merrill, L.; Barnett, J.D. A high pressure phase of cesium. *Science* **1964**, *146*, 1297–1299. [[CrossRef](#)] [[PubMed](#)]
43. Takemura, K.; Minomura, S.; Shimomura, O. X-ray Diffraction Study of Electronic Transitions in Cesium under High Pressure. *Phys. Rev. Lett.* **1982**, *49*, 1772–1775. [[CrossRef](#)]
44. Schwarz, U.; Takemura, K.; Hanfland, M.; Syassen, K. Crystal Structure of Cesium-V. *Phys. Rev. Lett.* **1998**, *81*, 2711–2713. [[CrossRef](#)]
45. Takemura, K.; Shimomura, O.; Fujihisa, H. Cs(VI): A new high-pressure polymorph of cesium above 72 GPa. *Phys. Rev. Lett.* **1991**, *66*, 2014–2017. [[CrossRef](#)] [[PubMed](#)]
46. Stinton, G.W.; MacLeod, S.G.; Cynn, H.; Errandonea, D.; Evans, W.J.; Proctor, J.E.; Meng, Y.; McMahon, M.I. Equation of state and high-pressure/high-temperature phase diagram of magnesium. *Phys. Rev. B* **2014**, *90*, 134105. [[CrossRef](#)]
47. Anzellini, A.; Errandonea, D.; MacLeod, S.G.; Botella, P.; Daisenberger, D.; De’Ath, J.M.; Gonzalez-Platas, J.; Ibáñez, J.; McMahon, M.I.; Munro, K.A.; et al. Phase diagram of calcium at high pressure and high temperature. *Phys. Rev. Mater.* **2022**, *2*, 083608. [[CrossRef](#)]
48. Anderson, M.S.; Swenson, C.A.; Peterson, D.T. Experimental equations of state for calcium, strontium, and barium metals to 20 kbar and from 4 to 295 K. *Phys. Rev. B* **1990**, *41*, 3329–3338. [[CrossRef](#)] [[PubMed](#)]
49. Olijnyk, H.; Holzapfel, W.B. Phase transitions in alkaline earth metals under pressure. *Phys. Lett. A* **1984**, *100*, 191–194. [[CrossRef](#)]
50. Fujihisa, H.; Nakamoto, Y.; Sakata, M.; Shimizu, K.; Matsuoka, T.; Ohishi, Y.; Yamawaki, H.; Takeya, S.; Gotoh, Y. Ca-VII: A Chain Ordered Host-Guest Structure of Calcium above 210 GPa. *Phys. Rev. Lett.* **2013**, *110*, 235501. [[CrossRef](#)]
51. Bovornratanaraks, T.; Allan, D.R.; Belmonte, S.A.; McMahon, M.I.; Nelmes, R.J. Complex monoclinic superstructure in Sr-IV. *Phys. Rev. B* **2006**, *73*, 144112. [[CrossRef](#)]
52. Nelmes, R.J.; Allan, D.R.; McMahon, M.I.; Belmonte, S.A. Self-Hosting Incommensurate Structure of Barium IV. *Phys. Rev. Lett.* **1999**, *83*, 4081–4084. [[CrossRef](#)]

53. Kenichi, T. High-pressure structural study of barium to 90 GPa. *Phys. Rev. B* **1994**, *50*, 16238–16246. [[CrossRef](#)] [[PubMed](#)]
54. Fujihisa, H.; Akahama, Y.; Kawamura, H.; Gotoh, Y.; Yamawaki, H.; Sakashita, M.; Takeya, S.; Honda, K. Incommensurate composite crystal structure of scandium-II. *Phys. Rev. B* **2005**, *72*, 132103. [[CrossRef](#)]
55. Stavrou, E.; Yang, L.H.; Söderlind, P.; Aberg, D.; Radousky, H.B.; Armstrong, M.R.; Belof, J.L.; Kunz, M.; Greenberg, E.; Prakapenka, V.B.; et al. Anharmonicity-induced first-order isostructural phase transition of zirconium under pressure. *Phys. Rev. B* **2018**, *98*, 220101. [[CrossRef](#)]
56. Anzellini, S.; Bottin, F.; Bouchet, J.; Dewaele, A. Phase transitions and equation of state of zirconium under high pressure. *Phys. Rev. B* **2020**, *102*, 184105. [[CrossRef](#)]
57. Akahama, Y.; Kawaguchi, S.; Hirao, N.; Ohishi, Y. High-pressure stability of bcc-vanadium and phase transition to a rhombohedral structure at 200 GPa. *J. Appl. Phys.* **2021**, *129*, 135902. [[CrossRef](#)]
58. Dewaele, A.; Torrent, M.; Loubeyre, P.; Mezouar, M. Compression curves of transition metals in the Mbar range: Experiments and projector augmented-wave calculations. *Phys. Rev. B* **2008**, *78*, 104102. [[CrossRef](#)]
59. Salamat, A.; Briggs, R.; Bouvier, P.; Petitgirard, S.; Dewaele, A.; Cutler, M.E.; Cora, F.; Daisenberger, D.; Garbarino, G.; McMillan, P.F. High-pressure structural transformations of Sn up to 138 GPa: Angle-dispersive synchrotron X-ray diffraction study. *Phys. Rev. B* **2013**, *88*, 104104. [[CrossRef](#)]
60. Kuznetsov, A.; Dmitriev, V.; Dubrovinsky, L.; Prakapenka, V.B.; Weber, H.-P. FCC–HCP phase boundary in lead. *Solid State Commun.* **2018**, *122*, 125–127. [[CrossRef](#)]
61. Mao, H.K.; Wu, Y.; Shu, J.F.; Hu, J.Z.; Hemley, R.J.; Cox, D.E. High pressure phase transition and equation of state of lead to 238 GPa. *Solid State Commun.* **1990**, *74*, 1027–1029. [[CrossRef](#)]
62. Degtyareva, O.; McMahon, M.I.; Allan, D.R.; Nelmes, R.J. Structural Complexity in Gallium under High Pressure: Relation to Alkali Elements. *Phys. Rev. Lett.* **2004**, *93*, 205502. [[CrossRef](#)] [[PubMed](#)]
63. Kenichi, T.; Kobayashi, K.; Arai, M. High-pressure bct-fcc phase transition in Ga. *Phys. Rev. B* **1998**, *58*, 2482–2486. [[CrossRef](#)]
64. Cazorla, C.; MacLeod, S.G.; Errandonea, D.; Munro, K.A.; McMahon, M.I.; Popescu, C. Thallium under extreme compression. *J. Phys. Condens. Matter* **2016**, *28*, 445401. [[CrossRef](#)] [[PubMed](#)]
65. Menoni, C.S.; Hu, J.Z.; Spain, I.L. Germanium at high pressures. *Phys. Rev. B* **1986**, *34*, 362–368. [[CrossRef](#)] [[PubMed](#)]
66. Takemura, K.; Schwarz, U.; Syassen, K.; Hanfland, M.; Christensen, N.E.; Novikov, D.L.; Loa, I. High-pressure Cmca and hcp phases of germanium. *Phys. Rev. B* **2000**, *62*, R10603–R10606. [[CrossRef](#)]
67. Kennedy, C.S.; Kennedy, G.C. Equilibrium boundary between graphite and diamond. *J. Geophys. Res.* **1976**, *81*, 2467–2470. [[CrossRef](#)]
68. McMahon, M.I.; Nelmes, R.J. New high-pressure phase of Si. *Phys. Rev. B* **1993**, *47*, 8337–8340. [[CrossRef](#)]
69. Hanfland, M.; Schwarz, U.; Syassen, K.; Takemura, K. Crystal Structure of the High-Pressure Phase Silicon VI. *Phys. Rev. Lett.* **1999**, *82*, 1197–1199. [[CrossRef](#)]
70. Akahama, Y.; Kawamura, H.; Carlson, S.; Le Bihan, T.; Hausermann, D. Structural stability and equation of state of simple-hexagonal phosphorus to 280 GPa: Phase transition at 262 GPa. *Phys. Rev. B* **2000**, *61*, 3139–3142. [[CrossRef](#)]
71. Degtyareva, O.; McMahon, M.I.; Nelmes, R.J. Pressure-induced incommensurate-to-incommensurate phase transition in antimony. *Phys. Rev. B* **2004**, *70*, 184119. [[CrossRef](#)]
72. Degtyareva, O.; Gregoryanz, E.; Mao, H.K.; Hemley, R.J. Crystal structure of sulfur and selenium at pressures up to 160 GPa. *High Press. Res.* **2005**, *25*, 17–33.
73. Hejny, C.; Falconi, S.; Lundegaard, L.F.; McMahon, M.I. Phase transitions in tellurium at high pressure and temperature. *Phys. Rev. B* **2006**, *74*, 174119. [[CrossRef](#)]
74. Akahama, Y.; Okawa, N.; Sugimoto, T.; Fujihisa, H.; Hirao, N.; Ohishi, Y. Coexistence of a metastable double hcp phase in bcc–fcc structure transition of Te under high pressure. *Jpn. J. Appl. Phys.* **2018**, *57*, 02560. [[CrossRef](#)]
75. Reichlin, R.; McMahan, A.K.; Ross, M.; Martin, S. Optical, X-ray, and band-structure studies of iodine at pressures of several megabars. *Phys. Rev. B* **1994**, *49*, 3725–3733. [[CrossRef](#)] [[PubMed](#)]
76. Fujihisa, H.; Takemura, K.; Onoda, M.; Gotoh, Y. Two intermediate incommensurate phases in the molecular dissociation process of solid iodine under high pressure. *Phys. Rev. Res.* **2021**, *3*, 033174. [[CrossRef](#)]
77. Vohra, Y.K.; Akella, J. 5f bonding in thorium metal at extreme compressions—Phase transitions to 300 GPa. *Phys. Rev. B* **1991**, *67*, 3563–3566.
78. Decremps, F.; Belhadi, L.; Farber, D.L.; Moore, K.T.; Ocelli, F.; Gauthier, M.; Polian, A.; Antonangeli, D.; Aracne-Ruddle, C.M.; Amadon, B. Diffusionless α - γ Phase Transition in Polycrystalline and Single-Crystal Cerium. *Phys. Rev. Lett.* **2011**, *106*, 065701. [[CrossRef](#)]
79. O'Bannon, E.F.; Pardo, O.S.; Soderlind, P.; Sneed, D.; Lipp, M.J.; Park, C.; Jenei, Z. Systematic structural study in praseodymium compressed in a neon pressure medium up to 185 GPa. *Phys. Rev. B* **2022**, *105*, 144107. [[CrossRef](#)]
80. Jayaraman, A.; Sherwood, R.C. Phase transformation in samarium induced by high pressure and its effect on the antiferromagnetic ordering. *Phys. Rev.* **1964**, *134*, A691–A692. [[CrossRef](#)]
81. Finnegan, S.E.; Pace, E.J.; Storm, C.V.; McMahon, M.I.; MacLeod, S.G.; Liermann, H.P.; Glazyrin, K. High-pressure structural systematics in samarium up to 222 GPa. *Phys. Rev. B* **2020**, *101*, 174109. [[CrossRef](#)]
82. Finnegan, S.E.; Storm, C.V.; Pace, E.J.; McMahon, M.I.; MacLeod, S.G.; Plekhanov, E.; Bonini, N.; Weber, C. High-Pressure Structural Systematics in Neodymium to 302 GPa. *Phys. Rev. B* **2021**, *103*, 134117. [[CrossRef](#)]

83. Husband, R.J.; Loa, I.; Munro, K.A.; McBride, E.E.; Evans, S.R.; Liermann, H.-P.; McMahon, M.I. Phase transitions in europium at high pressures. *High Press. Res.* **2013**, *33*, 158–164. [[CrossRef](#)]
84. Golosova, N.O.; Kozlenko, D.P.; Lukin, E.V.; Kichanov, S.E.; Savenko, B.N. High pressure effects on the crystal and magnetic structure of ¹⁶⁰Gd metal. *J. Magn. Magnet. Mater.* **2021**, *540*, 16848515. [[CrossRef](#)]
85. Errandonea, D.; Boehler, R.; Schwager, B.; Mezouar, M. Structural studies of gadolinium at high pressure and temperature. *Phys. Rev. B* **2007**, *75*, 014103. [[CrossRef](#)]
86. Tschauner, O.; Grubor-Urosevic, O.; Dera, P.; Mulcahy, S. Anomalous elastic behaviour in hcp-Sm-type Dysprosium. *J. Phys. Chem. C* **2012**, *116*, 2090–2095. [[CrossRef](#)]
87. Cerenius, Y.; Dubrovinsky, L. Compressibility measurements on iridium. *J. Alloys Comp.* **2000**, *306*, 26–29. [[CrossRef](#)]